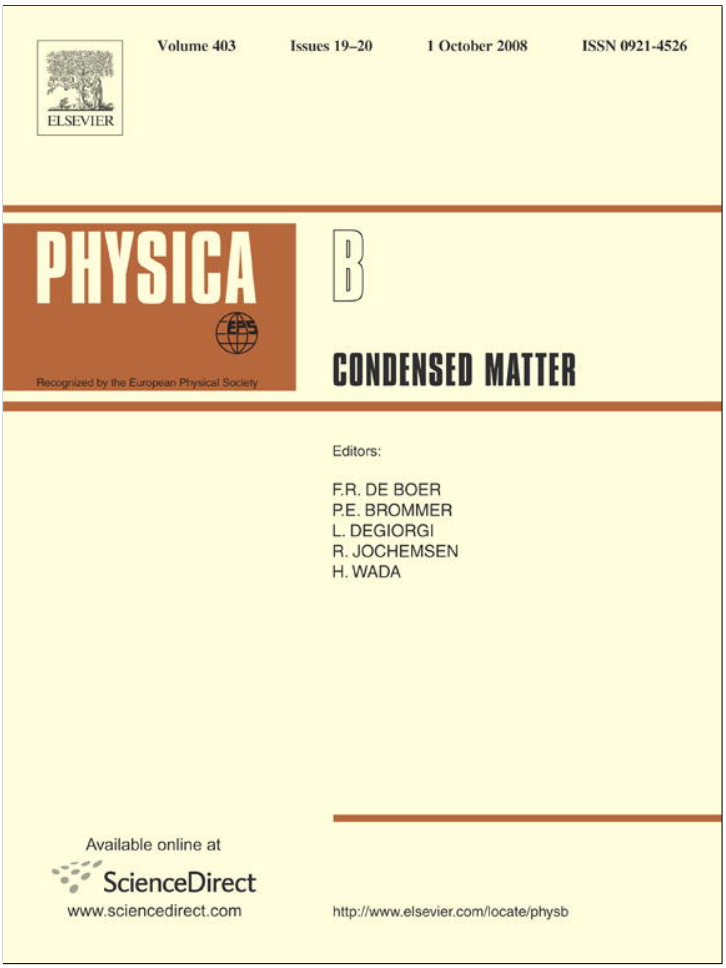

Physica B 403 (2008) 3559–3562

Contents lists available at ScienceDirect

Physica B

journal homepage: www.elsevier.com/locate/physb

First-principles calculation of vibrational Raman spectra of tetrahedral amorphous carbon

Li Niu *, Jiaqi Zhu *, Wei Gao, Aiping Liu, Xiao Han, Shanyi Du

Center for Composite Materials, Harbin Institute of Technology, No. 2 Yikuang Street, Nangang District, Harbin 150001, China

ARTICLE INFO

Article history:
Received 29 February 2008
Received in revised form
22 May 2008
Accepted 22 May 2008

PACS:
78.30.–j
71.15.Mb
81.05.Gc

Keywords:
Raman spectra
Density functional theory
Amorphous carbon

ABSTRACT

The nonresonant vibrational Raman spectra of tetrahedral amorphous carbon are calculated from first principles. The structural model was generated using Car–Parinello molecular dynamics, the vibrational modes are determined using the linear response approach and Raman tensors are calculated using the finite electric field method. Our theoretical visible and reduced Raman spectra show an overall good agreement with experimental spectra, and better than previous calculated results. The analysis in terms of atomic vibrations shows that the Raman spectrum mainly comes from sp^2 contribution, G peak is due to the stretching vibration of any pair of sp^2 atoms and only a small sp^3 contribution can be noticed. The differences between peak intensities of reduced theoretical and experimental results mainly come from defects and the high sp^3 content in our simulated structure.

1. Introduction

Tetrahedral amorphous carbon (ta-C) film is a hydrogen-free amorphous carbon (a-C) film containing sp^3 carbon bonding up to 85%. An increasing interest is to understand its atomic structure due to its superior mechanical, thermal, optical, electronic and tribological properties. Various characterization methods have been used to probe the key parameters that control its physical behavior, such as diffraction, electron energy loss spectroscopy, spectroscopic ellipsometry, X-ray photoelectron spectroscopy and Raman [1,2]. Raman spectroscopy is a relatively simple and nondestructive analysis tool [3,4] in these characterization methods. And it is very sensitive to the local structure in disordered materials [7], so is widely used. Since amorphous materials lack translational symmetry, all vibrational modes can contribute to Raman scattering intensity. Raman spectra of most amorphous carbons show a broad peak in the 800–2000 cm^{-1} region and can be decomposed into two broad features [8], the so-called G and D modes, which lie at around 1560 and 1360 cm^{-1}, respectively, for visible excitation. And an extra T peak, at around 1060 cm^{-1}, becomes visible only for UV excitation [4]. The G mode is due to the stretching vibration of any pair of sp^2 atoms [3]. The D mode is the breathing mode of sp^2 atoms in 6-member graphitic rings [2–4]. The T peak is due to the C–C sp^3 vibration [4–6].

The dispersion of peak positions and intensities with excitation wavelength or material structures is interesting and can be used to derive the information on sp^2 and sp^3 bonding in a-C. Visible Raman is sensitive only for the sp^2 sites, because of their much greater Raman scattering cross-section than sp^3 sites [9]. UV Raman spectroscopy, with a high photon energy of 5.1 eV, excites both the π and σ states, allowing a direct probe of the sp^3 bonding. Nevertheless, visible Raman spectroscopy is widely used on a-C [10–12]. An empirical three-stage model was well developed to relate the visible Raman spectra of carbon films to their local bonding [3]. However, an accurate theoretical modeling is necessary to understand more deeply the physical origin of the Raman spectra of a-C films and doped structures. The resonant Raman spectra of ta-C have already been obtained using a tight-binding approximation [5,6]. However, for the visible Raman spectrum the tight-binding approximation is not exact due to the existence of two peaks above 1300 cm^{-1}.

In this letter we perform, a fully first-principles calculation of nonresonant vibrational Raman spectra of ta-C. We compare our results to the experimental and calculated data and analyze the relationships between microscopic structures and vibrational features.

2. Theory and computational details

In a first-order Stokes process of Raman scattering, an incoming photon of frequency ω_L and polarization $\hat{e}_L$ gives an

* Corresponding authors. Tel.: +86 451 86402954; fax: +86 451 86417970.
E-mail addresses: niuli1978@yahoo.com.cn (L. Niu), zhujq@hit.edu.cn (J. Zhu).

0921-4526/$ - see front matter © 2008 Elsevier B.V. All rights reserved.
doi:10.1016/j.physb.2008.05.026

outgoing photon of frequency ω_S and polarization $\hat{e}_S$ and a vibrational excitation of frequency $\omega_n = \omega_L - \omega_S$. The Raman cross-section is given by [13]

$$\frac{d\sigma}{d\Omega} \sim \sum_n |\hat{e}_S \cdot R^n \cdot \hat{e}_L|^2 \frac{\hbar}{2\omega_n}[n(\omega_n)+1]\delta(\omega-\omega_n), \quad (1)$$

where $n(\omega_n)$ is Boson factor and R^n is the Raman tensor associated to the normal mode n

$$R^n_{ij} = \sqrt{V}\sum_{IK} \frac{\partial \chi_{ij}}{\partial r_{IK}} \frac{\xi^n_{IK}}{\sqrt{M_I}}, \quad (2)$$

where V is the volume of the sample, r_{IK} is the atomic position of atom I, M_I is the atomic mass, ξ^n_{IK} is the normalized vibrational eigenmode corresponding to the frequency ω_n, and χ_{ij} is the dielectric polarizability tensor.

Theoretically, the main difficulty of modeling the Raman spectrum is to calculate the Raman cross-section. To calculate this quantity, it is necessary to obtain a reliable structural model, its vibrational modes, frequencies and Raman coupling tensors. In this letter, the structural model was generated using Car–Parinello molecular dynamics (CPMD) [14], the vibrational modes and frequencies were determined using linear response [15,16], and Raman coupling tensors were calculated using the finite field approach [17] based on the density functional theory due to successful applications on the vibrational spectra of vitreous materials [18–20].

Then the dielectric polarizability tensor χ_{ij} is expressed as

$$\frac{\partial \chi_{ij}}{\partial r_{IK}} = -\frac{1}{V}\frac{\partial^2 F^{\varepsilon}_{IK}}{\partial \varepsilon_i \partial \varepsilon_j}\bigg|_0. \quad (3)$$

The F^{ε}_{IK} indicates the components of the atomic forces on the atom I in the presence of an electric field ε. The tensor $\partial\chi_{ij}/\partial r_{IK}$ may be calculated by taking second derivatives of the atomic forces with respect to the electric fields. The diagonal terms $\partial\chi_{ii}/\partial r_{IK}$ can be obtained by considering values for the electric field of $\varepsilon = 0, \pm h$, and by using the following 3-point formula:

$$\frac{\partial^2 F}{\partial^2 \varepsilon_i}\bigg|_0 \simeq \frac{1}{h^2}[F(-h) - 2F(0) + F(h)]. \quad (4)$$

The off-diagonal ($i \neq j$) term of $\partial\chi_{ij}/\partial r_{IK}$ is then given by

$$\frac{\partial^2 F}{\partial \varepsilon_i \partial \varepsilon_j}\bigg|_0 \simeq \frac{1}{4h'^2}[F(h',h') + F(-h',-h') - F(-h',h') - F(h',-h')] \quad (5)$$

where $h' = h/\sqrt{2}$. Using this method, we could obtain all the tensors $\partial\chi_{ij}/\partial r_{IK}$ by 19 selfconsistent minimizations of the electric-field-dependent energy functional and so calculate Raman coupling tensor R^n_{ij} (Eq. (2)). A detailed description of the methodology is given in Ref. [17].

The calculation of the contribution of the nth vibrational mode to the Raman spectrum requires taking the average of the tensors R^n_{ij} over all possible directions [13] because of the isotropic nature of disorder solids. This average can be expressed by means of the trace a and the anisotropy τ of the tensor R^n_{ij}. The two quantities are defined as (in the following we drop the index n for clarity)

$$a = (R_{11} + R_{22} + R_{33})/3$$
$$\tau^2 = [(R_{11} - R_{22})^2 + (R_{22} - R_{33})^2 + (R_{33} - R_{11})^2 + 6(R^2_{12} + R^2_{13} + R^2_{23})]/2.$$

Then, in a back-scattering geometry, the intensity of the Raman spectrum associated to the n mode is given by

$$I_{Ram} = a^2 + \frac{7\tau^2}{45}. \quad (6)$$

And the total Raman intensity is given by

$$I^P(\omega) = 4\pi \sum_n \frac{(\omega_L - \omega_n)^4 V}{c^4} I^n_{Ram} \frac{\hbar}{2\omega_n}[n(\omega_n)+1]\delta(\omega-\omega_n). \quad (7)$$

The Raman spectra of disordered solids are usually discussed in terms of the so-called reduced spectrum I_{red}, which is obtained by

$$I^P_R(\omega) = \omega(\omega_L - \omega_n)^{-4}[n(\omega)+1]^{-1} I^P(\omega). \quad (8)$$

The final Raman spectra to be compared with experimentally measured spectra are obtained by uniform Gaussian broadening of calculated Raman intensities, which takes into account both experimental width of the Raman line and the finite size of our model.

We calculated nonresonant vibrational Raman spectra of a realistic model of ta-C generated by the liquid-quench method using CPMD as described elsewhere [21]. The geometry optimization and all calculations were performed within the framework of the density functional theory (DFT) within the local density approximation (LDA) and norm-conserving pseudopotentials in Troullier–Martin type, as provided in the QUANTUM-ESPRESSO package [22]. We adopted cutoff energies of 55 Ry for the plane-wave functions, applied electric fields of $h = 0.001$ a.u. and the Brillouin zone of the cell was sampled only at the Γ point.

3. Results and discussion

Fig. 1 shows a ball and stick model of ta-C in a cell. The simulated model contains 64 carbon atoms at the experimental density (3.2 g/cm^3) in a periodically repeated cubic cell. Among the 64 atoms, 10 atoms are threefold coordinated (sp^2 hybridized) and the others are fourfold coordinated (sp^3 hybridized). The sp^2 atoms are arranged in three pairs, a three-atom chain and an isolated atom which exists in a three-membered ring. The defects are the sites with odd numbered sp^2 atoms.

We first analyzed the vibrational density of states (v-DOS), which underlies all the vibrational spectra. By using the linear response method we derived the $3N$ eigenfrequencies ω_n and their corresponding normalized eigenmodes ξ^n_{IK}. The normalized v-DOS

$$G(\omega) = \frac{1}{3N}\sum_n \delta(\omega - \omega_n) \quad (9)$$

is shown in Fig. 2, where a Gaussian broadening with $\sigma = 50\,\text{cm}^{-1}$ is used. The v-DOS is decomposed according to the weights of the eigenmodes on the sp^3 and sp^2 sites, according to $G(\omega) = \sum_\alpha G_\alpha(\omega)$, where the partial density of states $G_\alpha(\omega)$ is defined by

$$G_\alpha(\omega) = \frac{1}{3N}\sum_I^{N_\alpha}\sum_n |\xi^n_I|^2 \delta(\omega - \omega_n). \quad (10)$$

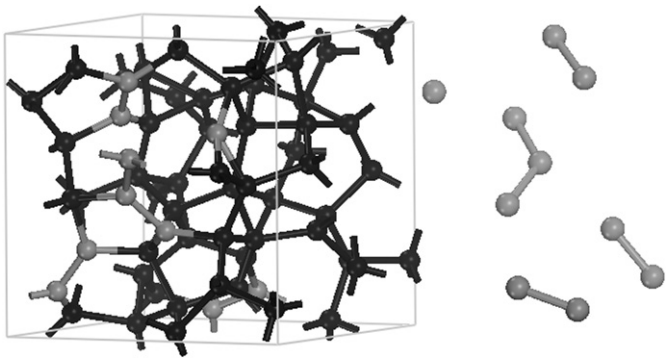

Fig. 1. Ball and stick model of the simulated ta-C. Black and gray atoms denote sp^3 and sp^2 sites, respectively.

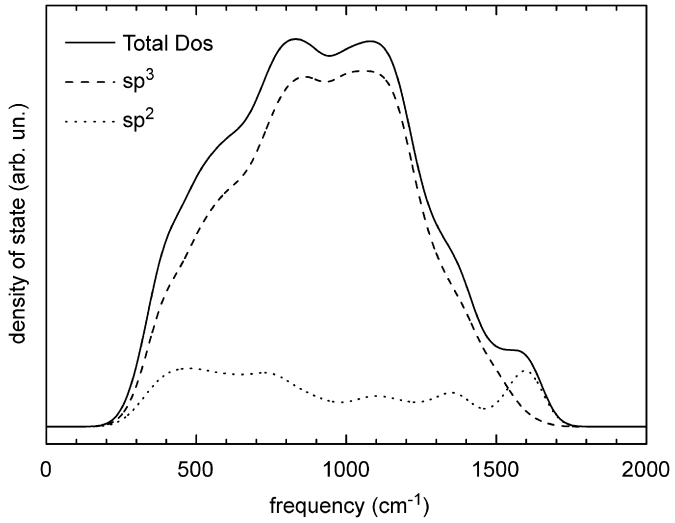

Fig. 2. The calculated total (solid line) and partial v-DOS of ta-C. The v-DOS is decomposed into the contributions of the sp^3 carbon atoms (dashed line) and sp^2 carbon atoms (dotted line).

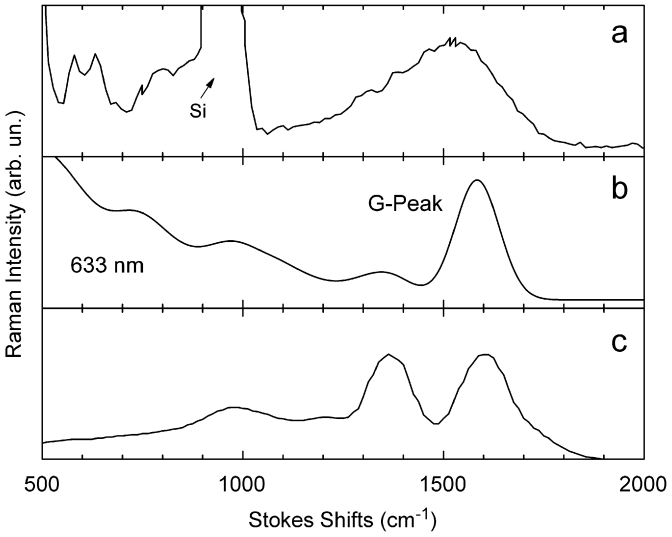

Fig. 3. Calculated visible Raman spectrum of ta-C in 633 nm (b) compared with the experimental data of Ref. [4] (a) and the calculated data of Ref. [6] (c). A Gaussian broadening of 50 cm^{-1} is used in our theoretical spectrum.

The sum over I is over all the atoms belonging to α species. Fig. 2 shows that the sp^2 vibrations are dominant in the entire range of frequencies, while the sp^3 vibrations clearly dominate the total v-DOS and die over 1500 cm^{-1}. Thus, the modes above 1500 cm^{-1} involve only sp^2 carbons. Similar theoretical results have been presented in Refs. [5,6] and show the reliability of our model.

The nonresonant vibrational Raman intensities should be compared with measures done using long-wavelength incident light. In Fig. 3, we compared the calculated visible Raman spectroscopy of the ta-C network in the 633 nm with the measured nonpolarized Raman spectrum taken from Ref. [4] and the theoretical data taken from Ref. [6]. Despite theoretical simplicity, our model reproduces well the observed vibrational Raman spectrum and better than the previous calculated results. At low frequencies, the Raman spectrum is enhanced because at room temperature there is a greater population of the thermally excited low-energy phonons with which to interact.

We hereafter focused on the reduced Raman spectra, which remove extraneous temperature dependencies and thus better highlight the dependence on the coupling tensors. In Fig. 4, the calculated reduced Raman spectrum is compared to available experimental data [23]. Since the experimental spectrum is given on a relative scale, we rescale the theoretical one by a constant factor to match the integrated intensity of the experimental spectrum. The agreement is excellent. Apart from small differences in peak intensities, the calculated spectrum reproduces well the location of the principal peaks. The differences between theoretical and corresponding experimental intensities are due to different sp^2/sp^3 ratio in structures.

With respect to their experimental counterparts, the simulated Raman spectra offer the advantage that they conveniently be analyzed in terms of the underlying vibrational modes. Fig. 5(a) gives the decomposition of the reduced Raman spectrum into sp^3 and sp^2 weights. This decomposition is achieved by selecting the components of the vibrational eigenmodes specific to either sp^3 or sp^2 prior to the calculation of the Raman intensities. While the components obtained in this way do not sum up to give the full spectrum because of the interference terms, this analysis nevertheless provides insight into the origin of the various features. We see even if our ta-C model has a high 84.4% sp^3 fraction, the Raman intensity mainly comes from sp^2 carbon atoms contribution. This clearly proves that the G peak at 1582 cm^{-1}, which is the main features of the ta-C spectrum, is entirely due to vibrations of sp^2 atoms. At the medium part of the spectrum the sp^3 contribution exceeds the sp^2 contribution, and the sp^3 vibrations give rise to a small peak centered at 1000 cm^{-1} which is called T peak.

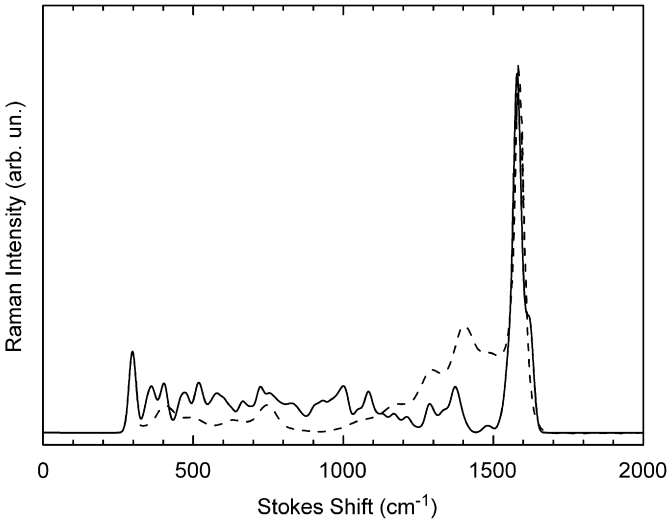

Fig. 4. Calculated reduced Raman spectrum of ta-C (solid line) compared with the experimental data of Ref. [23] (dashed line). A Gaussian broadening of 12 cm^{-1} is used.

The contribution of sp^2 atoms is further analyzed in Fig. 5(b) in terms of paired atoms, the three-atom chain and the isolated atom. The decomposition on these atoms shows that the low-frequency peak at 351 cm^{-1} mainly comes from the contribution of the isolated sp^2 atom. This suggests that the differences between the intensity of reduced theoretical and experimental results in the low-frequency region should be attributed to defects in our simulated structure. And the decomposition further proves G peak is due to the stretching vibration of any pair of sp^2 atoms.

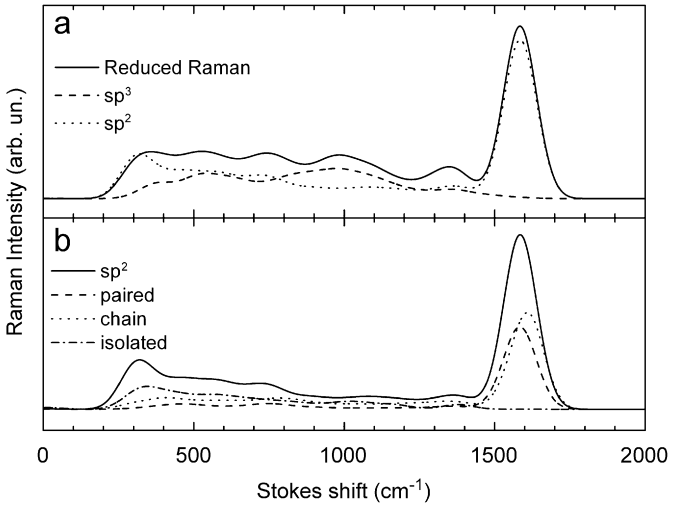

Fig. 5. (a) The calculated reduced Raman spectrum (solid line) and partial contributions of sp^3 carbon atoms (dashed line) and sp^2 carbon atoms (dotted line). (b) Further decomposition of the sp^2 weight into paired atoms (dashed line), a three-atom chain (dotted line) and the isolated atom (dash-dotted line).

4. Conclusions

In summary, nonresonant vibrational Raman spectra of ta-C was calculated within a fully density-functional scheme, including the generation of structural model, the calculation of vibrational frequencies, eigenmodes and Raman coupling tensors. Our results show an overall good agreement with experimental data. The analysis in terms of atomic vibrations shows that the Raman spectrum mainly comes from sp^2 carbons contribution and G peak is the stretching vibration of paired sp^2 atoms. Only a small T peak can be noticed. The differences between the intensity of reduced theoretical and experimental results come from defects of odd sp^2 atoms and the high sp^3 content in our simulated structure.

Acknowledgments

This work was supported by the National Natural Science Foundation of China (50602012) and the Science Creative Foundation for Distinguished Young Scholars in Harbin (2007RFQXG039).

References

[1] Y. Lifshitz, Diamond Relat. Mater. 8 (1999) 1659.
[2] J. Robertson, Math. Sci. Eng. R 37 (2002) 129.
[3] A.C. Ferrari, J. Robertson, Phys. Rev. B 61 (2000) 14095.
[4] A.C. Ferrari, J. Robertson, Phys. Rev. B 64 (2001) 075414.
[5] M. Profeta, F. Mauri, Phys. Rev. B 63 (2001) 245415.
[6] S. Piscanec, F. Mauri, A.C. Ferrari, M. Lazzeri, J. Robertson, Diamond Relat. Mater. 14 (2005) 1078.
[7] P. Umari, A. Pasquarello, Physica B 316 (2002) 572.
[8] M.A. Tamor, W.C. Vassell, J. Appl. Phys. 76 (1994) 3823.
[9] N. Wada, S.A. Solin, Physica B 105 (1981) 353.
[10] J.R. Shia, J. Appl. Phys. 99 (2006) 033505.
[11] L. Zeng, E. Helgren, F. Hellman, R. Islam, D.J. Smith, J.W. Ager III, Phys. Rev. B 75 (2007) 235450.
[12] M.L. Tan, J.Q. Zhu, J.C. Han, W. Gao, A.P. Liu, X. Han, Mater. Res. Bull. 43 (2008) 453.
[13] Light Scattering in Solids II, M. Cardona, G. Güntherod (Eds.), Springer, Berlin, 1982.
[14] N.A. Marks, D.R. McKenzie, B.A. Pailthorpe, M. Bernasconi, M. Parrinello, Phys. Rev. Lett. 76 (1996) 768.
[15] P. Giannozzi, S. de Gironcoli, P. Pavone, S. Baroni, Phys. Rev. B 43 (1991) 7231.
[16] S. Baroni, S. de Gironcoli, A. Dal Corso, P. Giannozzi, Rev. Mod. Phys. 73 (2001) 515.
[17] P. Umari, A. Pasquarello, Diamond Relat. Mater. 14 (2005) 1255.
[18] P. Umari, A. Pasquarello, Phys. Rev. Lett. 95 (2005) 137401.
[19] L. Giacomazzi, P. Umari, A. Pasquarello, Phys. Rev. B 74 (2006) 155208.
[20] L. Giacomazzi, C. Massobrio, A. Pasquarello, Phys. Rev. B 75 (2007) 174207.
[21] J.C. Han, W. Gao, J.Q. Zhu, S.H. Meng, W.T. Zheng, Phys. Rev. B 75 (2007) 155418.
[22] S. Baroni, A. Dal Corso, S. de Gironcoli, P. Giannozzi, 〈http://www.pwscf.org〉.
[23] Q. Wang, D.D. Allred, J. Gonza′lez-Herna′ndez, Phys. Rev. B 47 (1993) 6119.